JMEPEG (2010) 19:700–704
DOI: 10.1007/s11665-009-9550-3

1059-9495/$19.00

High Temperature Mechanical Properties of HK40-type Heat-resistant Cast Austenitic Stainless Steels

Yoon-Jun Kim, Dong-Geun Lee, Hyeon Kyeong Jeong, Yong-Tai Lee, and Ho Jang

(Submitted January 2, 2009; in revised form August 26, 2009)

This work characterized HK40-type, cast austenitic stainless steel, as the W content was varied from 0 to 3.6 wt.%. Analysis of microstructure using optical and scanning electron microscopies showed that the alloys contained relatively large amount of Cr-carbide, Nb-compound, and MnS at the austenite grain boundary. The addition of W promoted the formation of Cr-carbide and affected the high-temperature mechanical properties. According to tension tests carried out at room temperature, 400, 600, and 800 °C, the alloys became significantly stronger and brittle as W content increased. The low-cycle fatigue tests showed that fatigue resistance was also increased with W addition, but an excessive amount of W decreased the fatigue resistance. The HK40-type alloys with 2.0 wt.% W exhibited best high-temperature mechanical performances.

Keywords heat resistant steels, intermetallic phase, low-cycle fatigue, stainless steels, tensile strength

1. Introduction

Cast austenitic stainless steels are one of the most popular heat-resistant alloys used for high-temperature applications (Ref 1) which require high strength and thermal fatigue life at elevated temperature. These high-temperature mechanical properties of stainless steels are highly dependent upon alloying additions. Numerous studies have been undertaken to examine the phase transformation behavior and associated effects of alloying elements and mechanical properties of various types of wrought austenitic stainless steels (Ref 2-5). Alloying elements such as W, Mo, Nb, V, and N have been reported to be effective in strengthening stainless steels at elevated temperatures. In general, precipitation hardening takes place in stainless steels alloyed with the above elements except W, which is known to act as a solid solution strengthening element (Ref 2).

However, even though both wrought and cast austenitic stainless steels are used in many high-temperature applications such as automotive exhaust systems and power plants, cast steels have received little research attention. It should be expected that the mechanical properties at elevated temperatures are different between cast and wrought alloys due to differences in their nominal compositions and their microstructures. Unlike wrought stainless steels, cast stainless steels contain relatively high C and Si contents in order to increase fluidity. Furthermore, castings usually show a dendritic microstructure due to fast cooling after pouring. Therefore, alloying effects may cause different phase equilibria and mechanical properties from those seen in wrought alloys.

The aim of this article is to investigate the high-temperature tensile properties and the microstructural evolution for HK40-type, cast austenitic stainless steels. Although this type of steel had been studied by other researchers (Ref 6-8), the high-temperature mechanical properties have been scantily researched. However, those properties are the most important factors affecting the durability of the high-temperature applications under thermal shock loading.

2. Experimental Procedures

The materials used in this experiment were based on the ACI (Alloy Casting Institute which is currently administered by the High Alloy Product Group of the Steel Founders' Society of America) HK40 grade, heat-resistant, cast stainless steel. This alloy contains as much as 2.5 wt.% Nb in order to increase the high-temperature stability. Three different alloys with varying W content were used in the experiments and the chemical composition of each sample is given in Table 1.

The steel specimens were cast in the form of Y-blocks of approximate dimensions 50 × 200 × 100 mm, which were then cut into small coupons of dimensions 20 × 30 × 100 mm. Specimens for elevated temperature tension tests were machined from those coupons. Cylindrical specimens with a diameter of 6 mm and a gauge length of 25 mm were prepared in accordance with the ASTM E21 standard (Ref 9). The tension test was carried out at four different temperatures, room temperature, 400, 600, and 800 °C, at a constant cross head speed of 2.0 mm/min. At each temperature, minimum three specimens were tested and their yield strengths (YS, alternatively called the 0.2% proof strength), ultimate tensile strengths (UTS), and total elongations were obtained. The low-cycle

Yoon-Jun Kim and **Ho Jang**, Department of Materials Science and Engineering, Korea University, Anam-dong, Seongbuk-gu, Seoul 136-701, Korea; and **Dong-Geun Lee, Hyeon Kyeong Jeong,** and **Yong-Tai Lee**, Korea Institute of Materials Science, 531 Changwondaero, Changwon 641-831, Korea. Contact e-mails: yoonjun@korea.ac.kr and hojang@korea.ac.kr.

Table 1 Measured chemical compositions (wt.%) of the HK40-type alloys

	C	Si	Mn	P	S	Ni	Cr	Nb	W
A1	0.56	0.97	1.13	0.026	0.215	18.85	25.12	2.52	…
A2	0.53	1.31	1.10	0.028	0.218	19.44	25.61	2.46	2.04
A3	0.54	1.09	1.20	0.029	0.216	19.69	25.59	2.51	3.60

fatigue (LCF) tests were conducted using a servo hydraulic machine equipped with a heating furnace. The test was carried out at the maximum temperature used for the tension tests, i.e., 800 °C. The input total strain ranges ($\Delta\varepsilon$) were in the range from ±0.3% to ±0.5%, and the strain rate was 1.4×10^{-3} per second. The strain wave form was a symmetric triangle with a load ratio of $R = -1$. Each sample located inside a furnace was heated rapidly and held for at least 30 min at the test temperatures prior to applying load. It was assumed that this time was sufficient for a uniform test temperature to be reached, and for the structure in the center region, where the strain gauge was located, to be dissolved and homogenized.

Metallographic cross sections were prepared using standard techniques. The polished samples were etched using a Glyceregia-based solution consisting of 45 mL Glycerin + 30 mL Hydrochloric acid + 15 mL nitric acid (Ref 10). Optical and scanning electron microscopies (SEM) were used for the microstructural characterization. For the SEM analyses, images were taken at the accelerating voltage of 20 kV, and the chemical compositions of the phases were determined using an energy dispersive spectrometer (EDS).

3. Results and Discussion

Metallographic examination of the as-cast samples confirmed that austenitic matrix was dendritic. In addition, some of the secondary phases such as eutectoid- and needle-like precipitates were formed in the interdendritic region, suggesting that this phase assemblage developed by a combination of austenite and precipitates formed at high temperatures at prior austenite grain boundaries during casting. A typical optical micrograph of the cast austenitic stainless steel is shown in Fig. 1. In spite of different W contents in the steels, the three samples showed almost same volume percents and shapes of precipitates based on the optical microscopy.

The effect of W addition on the microstructural evolution was observed by measuring chemical compositions of the major phases using SEM equipped with EDS. The EDS results were taken from the austenite matrix and variously shaped secondary phases such as eutectoid-like, needle-like, and small globular shapes denoted in Fig. 1 as (1), (2), (3), and (4), respectively. Austenite matrices for the three alloys were very similar in Fe, Ni, and Cr contents, while no Nb or W was detected. Precipitates in the interdendritic region were also investigated. First, needle-shaped phase which has thin plate with 1.64 μm thickness, consists of mostly Nb with small amounts of Fe, Cr, and Ni. Apparently, Nb atoms were removed from the austenite matrix and precipitated in the interdendritic region as Nb-compound. Neither the matrix nor the Nb compound contains W. Secondly, eutectoid-like precipitates have very high Cr content with varying W content. The grain size and volume percent of this high Cr-precipitate were

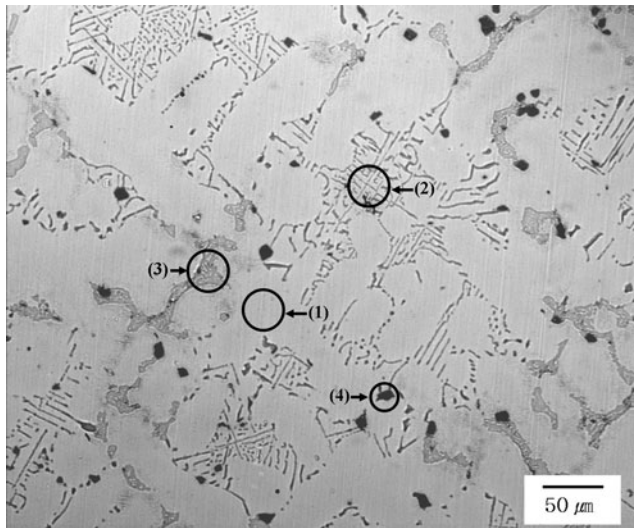

Fig. 1 Typical micrographs of the cast austenitic steel comprising four different phases: (1) austenite matrix, (2) Nb-compound, (3) Cr-carbide, and (4) MnS. The chemical composition of each phase was identified using EDS, as shown in Table 2

measured into 23.1 μm and 6.9 vol.%, respectively. The precipitates in the A1 alloy do not contain W, whereas those in the A2 and A3 alloys contain 9.45 and 16.44 wt.% W, respectively. Although EDS analysis did not produce accurate quantitative data, this phase was attributed to a high Cr-carbide (Ref 8). Finally, small globular shaped MnS was identified and measured to be 9.3 μm in grain size, which was precipitated homogeneously in whole matrix region, adjacent to Nb compound or high Cr-precipitate with 1.4 vol.%. This phase is more favorable to a better machinability than to strengthening those steels. The x-ray spectra obtained from these phases in each alloy are summarized in Table 2.

Figure 2 shows the typical stress-strain curves for the A2 alloy, and similar curves were obtained for other alloys. Work hardening occurred from room temperature up to 600 °C but both YS and UTS decreased with increasing test temperature. At 800 °C, the material was obviously softened because both YS and UTS were substantially decreased and the strain was greatly increased. The other two alloys exhibited the same tendency.

The YS, UTS, and total elongation at elevated temperatures are plotted in Fig. 3. The YS exhibited a similar tendency throughout the examined temperatures in all three alloys, as shown in Fig. 3(a). The strength decreased with increasing test temperature. The highest YS of the A1, A2, and A3 alloys were obtained at room temperature, which were 320, 304, and 327 MPa, respectively. At 400 and 600 °C, those specimens tended to maintain similar YS. However, the YS significantly dropped to less than 200 MPa, when the temperature was raised to 800 °C. In accordance with alloy addition effect, the YS increased with increasing W content at each test temperature but its difference was not significant with a range of only 20 MPa.

As shown in Fig. 3(a), the UTS exhibited a similar tendency to the YS from room temperature up to 600 °C. However, at 800 °C, the UTS for A1 and A2 alloys were more significantly decreased as compared to the A3 alloy. At this temperature, these UTS were 204, 222, and 246 MPa for A1, A2, and A3

Table 2 Average compositions (wt.%) of the austenite, Nb-compound, Cr-carbide, and MnS phases in the A1, A2, and A3 alloys

Alloys	Phases	Fe	Cr	Ni	Nb	W	Mn	Si	S
A1	(1) Austenite	54.19	22.85	20.52	…	…	1.11	1.33	
	(2) Nb-compound	3.30	2.60	1.23	92.87	…	…	…	
	(3) Cr-carbide	14.31	82.30	2.66	…	…	…	0.73	
	(4) MnS	…	24.62	…	…	…	37.69	…	37.70
A2	(1) Austenite	51.82	23.93	21.70	…	…	0.90	1.65	
	(2) Nb-compound	1.55	1.69	0.67	95.87	…	…	…	
	(3) Cr-carbide	9.13	80.46	0.96	…	9.45	…	…	
	(4) MnS	…	25.05	…	…	…	38.01	…	36.94
A3	(1) Austenite	50.27	24.62	22.14	…	…	1.09	1.88	
	(2) Nb-compound	2.81	3.45	1.18	92.56	…	…	…	
	(3) Cr-carbide	29.22	41.38	12.32	…	16.44	…	0.63	
	(4) MnS	…	21.51	…	…	…	40.84	…	37.65

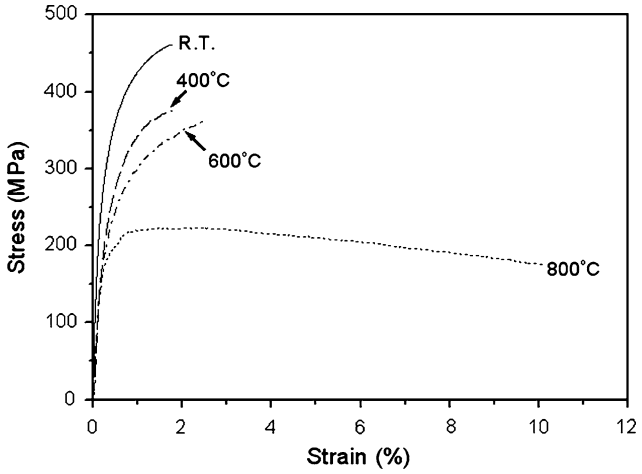

Fig. 2 Stress-strain curves for A2 alloy tested at room temperature, 400, 600, and 800 °C

alloys, respectively. The difference between the A1 and A3 alloys was 42 MPa, which is obviously greater than that of YS. The variation in W content exerted greater influence over UTS rather than YS at high temperatures, especially for the 800 °C samples.

The total elongations shown in Fig. 3(b) for the three alloys were not substantially increased as the temperature was raised from room temperature to 600 °C. Alloys A1 and A2 showed similar elongation in this range, whereas A3 showed slightly lower elongation. However, the elongations at 800 °C for all alloys were abruptly increased. At this temperature, the elongation varied significantly among the three alloys, and was 19.6, 17.5, and 14.6% for A1, A2, and A3 alloys, respectively. The alloy with the highest W content, the A3, exhibited 5% less elongation than the A1 alloy.

In addition, the low-cycle fatigue life was dependent on the W content. Figure 4 shows the number of cycles to failure (N_f) as a function of applied plastic strain range ($\Delta\varepsilon_p$) at 800 °C. At high plastic strain ranges ($\Delta\varepsilon_p$ = 0.30%), A1 showed a longer fatigue life than others. However, the fatigue life of A2 became the longest among tested alloys if $\Delta\varepsilon_p$ = 0.30%. The A3 alloy which contains the highest W content shows inferior LCF property. It is also found that plotting $\Delta\varepsilon_p$ to N_f in logarithmic scale appeared essentially a straight line, and can be described by the well-known Coffin-Manson equation (Ref 11, 12):

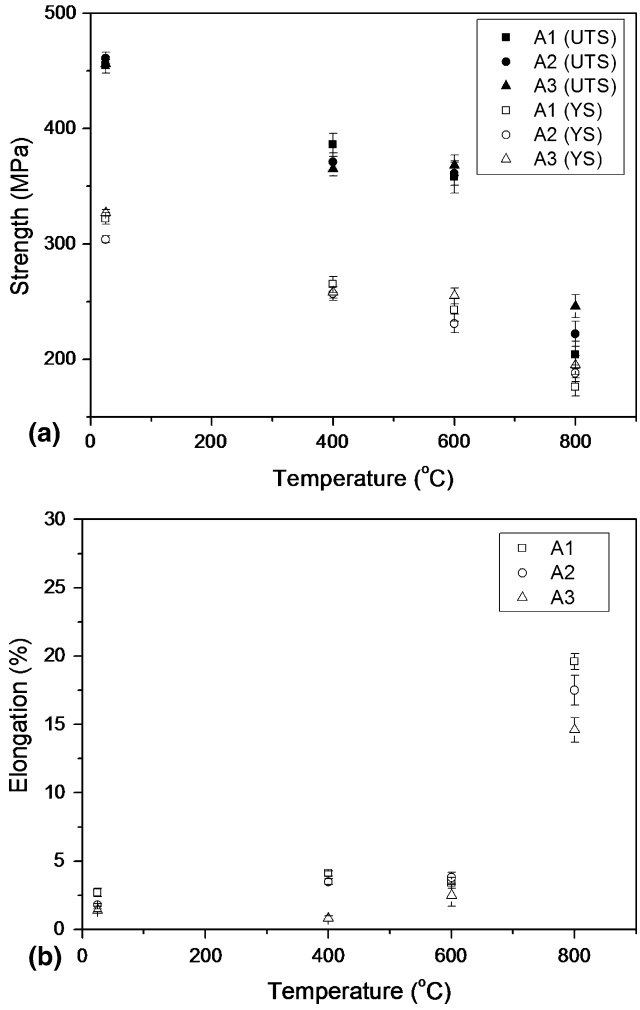

Fig. 3 Tensile properties of the A1, A2, and A3 alloys: (a) YS and UTS, and (b) total elongation

$$\frac{\Delta\varepsilon_p}{2} = \varepsilon_f'(2N_f)^c \quad \text{(Eq 1)}$$

where $\Delta\varepsilon_p/2$ is the cyclic plastic strain amplitude, ε_f' is the fatigue ductility coefficient, $2N_f$ is the number of strain reversal to failure, and c is the fatigue ductility exponent. The

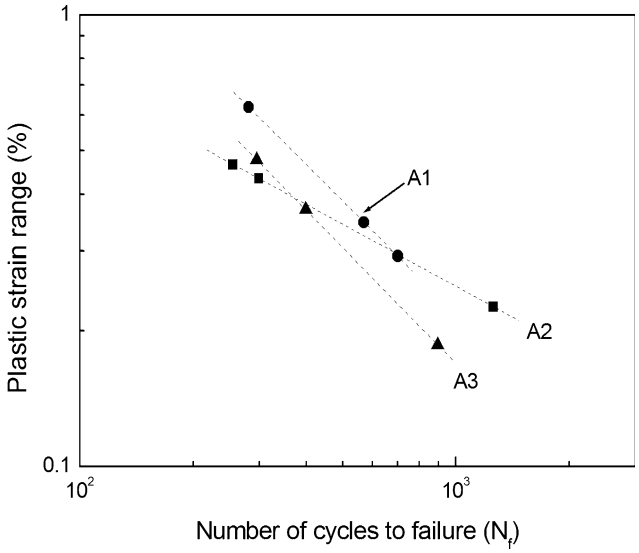

Fig. 4 Fatigue lives vs. plastic strain range of A1, A2, and A3 alloys

Table 3 Fatigue exponents in Eq (1) for A1, A2, and A3 alloys at 800 °C

Alloys	c	ε_f'
A1	−0.831	0.602
A2	−0.452	0.039
A3	−0.848	0.534

exponents, ε_f' and c, are calculated from Fig. 4 and summarized in Table 3. It is noted that the slope of log $\Delta\varepsilon_p$ versus N_f curve indicates the fatigue ductility exponent, c in Eq (1). This exponent for A2 is approximately a half of both A1 and A3 alloys, suggesting that the A2 alloy shows low sensitivity of different input plastic strains.

Disparity in the effect of W addition between the results in tensile and LCF tests was found. The tension test results indicated that the W addition obviously strengthened the alloys, especially at elevated temperature such as 800 °C. However, the excessive amount of W did not improve LCF property, and therefore, the optimum W content should be around 2.0 wt.%. Such a fatigue behavior of those alloys can be understood by comparing YS and elongation. If the alloy possesses higher YS and similar uniform elongation, and if the same input strain amplitude is applied, stress concentration at around grain boundary increased. Therefore, fatigue failure for A3 may occur at shorter time in spite of higher YS and UTS due to more addition of W.

Both tensile and fatigue properties of cast austenitic stainless steels rely on the precipitation of secondary phases, especially Cr-rich carbide as indicated in Table 2. It had been reported for various types of wrought stainless steels that the Cr-rich phases such as Cr-carbide is very hard and brittle phases, which can be precipitated at high temperature, usually above 600 °C (Ref 10). The formation of this phase increases the strength but reduces the ductility. It is found from this study that the W addition can promote Cr-carbide formation. Such a phase was more stabilized in the W-added steels. The resulting mechanical properties at 800 °C showed higher YS and UTS, and lower elongation with increasing W content. Therefore, the A3 alloy became strong and brittle compared to the alloys containing lower W content. However, the excessive W addition was not beneficial to LCF property. Therefore, the A1 alloy was found to be suitable for high temperature applications because of its best combination of strength and fatigue resistance.

4. Conclusions

The microstructure of ACI HK40-type, cast austenitic stainless steels consisted of austenite matrix, Nb-compound, Cr-carbide, and MnS. Tungsten was detected only in the Cr-carbide and may promote the formation of this phase. Since carbide formation was affected by the W content, the addition of W increased the strength but reduced the ductility. The optimum W content in terms of tensile strength and low-cycle fatigue resistance was about 2.0 wt.%.

Acknowledgments

This work was supported partly by the Materials & Components Technology Development program funded by the Korean Ministry of Knowledge Economy, and partly by the Korea Science and Engineering Foundation (KOSEF) through the National Research Lab. Program funded by the Ministry of Science and Technology (No. R0A-2007-000-10011-0).

References

1. P.Y. Chen, R. Lyons. M. Rakoczy, K. Otsuka, H. Yamanaka, and T. Mimata, Development of the 6.8L V10 Heat Resisting Cast-Steel Exhaust Manifold, *SAE 1996 World Congress*, Detroit, MI, Oct 1996, Paper No. 962169
2. T. Ishitsuka and H. Mimura, Development of 18Cr-9Ni-W-Nb-V-N Austenitic Stainless Steel Tube for Thermal Power Boilers, *JSME Int. J.*, 2002, **45**(1), p 110–117
3. Y. Hosoi, Y. Shimoide, M. Abraham, M. Kutsuna, and K. Miyahara, Influence of Tungsten Carbon and Nitrogen on Toughness and Weldability of Low Activation Austenitic High Managese Stainless Steels, *J. Nucl. Mater.*, 1992, **191-194**, p 686–690
4. Y. Yamamoto, M.P. Brady, Z.P. Lu, C.T. Liu, M. Takeyama, P.J. Maziasz, and B.A. Pint, Alumina-Forming Austenitic Stainless Steels Strengthened by Laves Phase and MC Carbide Precipitates, *Metall. Mater. Trans. A*, 2007, **38**(11), p 2737–2746
5. R.L. Klueh and P.J. Maziasz, Tensile and Microstructural Behavior of Solute-modified Manganese-stabilized Austenitic Steels, *Mater. Sci. Eng. A*, 1990, **127**(1), p 17–31
6. E. Otero, A. Pardo, F.J. Perez, J.F. Alvarez, and M.V. Utrilla, A High Temperature Corrosion Kinetic Study of HK-40 Superalloy Surface Treated, in Contact with Eutectic Mixture 82%$K_2S_2O_7$-18%V_2O_5, *Corros. Sci.*, 1997, **39**(1), p 133–145
7. C. Cuevas-Arteaga, J. Uruchurtu-Chavarin, J. Porcayo-Calderon, G. Izquierdo-Montalvo, and J. Gonzales, Study of Molten Salt Corrosion of HK-40m Alloy Applying Linear Polarization Resistance and Conventional Weight Loss Techniques, *Corros. Sci.*, 2004, **46**(11), p 2663–2679
8. F.C. Nunes, L.H. de Almeida, and A.F. Ribeiro, Correlation Between Molten Vanadium Salts and the Structural Degradation of HK-Type Steel Superheater Tubes, *J. Mater. Eng. Perform.*, 2006, **15**(6), p 717–721

9. "Standard Test Method for Elevated Temperature Tension Tests of Metallic Materials," E21-92, *Annual Book of ASTM Standards*, vol. 03.01, ASTM, p 136–143
10. J.R. Davis, Ed., *ASM Specialty Handbook-Stainless Steels*, ASM International, Materials Park, Ohio, 1994
11. L.F. Coffin, A Study of the Effects of Cyclic Thermal Stresses on a Ductile Metal, *Trans. ASME*, 1954, **76**, p 931–950
12. G.H. Rubiolo, Temperature and Strain Rate Superposition Properties of Low Cycle Fatigue Failure Curves in the Coffin-Manson Representation, *Acta Metall. Mater.*, 1991, **39**(4), p 619–626